

# Investigation of Oxide Thermoelectrics based on Indium and Tin



A thesis submitted towards partial fulfilment of  
BS-MS Dual Degree Programme

by

DEVIKA T D

under the guidance of

DR. SUNIL NAIR

ASSISTANT PROFESSOR

INDIAN INSTITUTE OF SCIENCE EDUCATION AND RESEARCH PUNE

# Certificate

This is to certify that this thesis entitled "Investigation of Oxide Thermoelectrics based on Indium and Tin" submitted towards the partial fulfilment of the BS-MS dual degree programme at the Indian Institute of Science Education and Research Pune represents original research carried out by "Devika T D" at "Indian Institute of Science Education and Research Pune", under the supervision of "Dr. Sunil Nair" during the academic year 2015-2016.

Student  
DEVIKA T D





Supervisor  
DR. SUNIL NAIR



# Declaration

I hereby declare that the matter embodied in the report entitled "Investigation of Oxide Thermoelectrics based on Indium and Tin" are the results of the investigations carried out by me at the Department of Physics, Indian Institute of Science Education and Research Pune, under the supervision of Dr. Sunil Nair and the same has not been submitted elsewhere for any other degree.

Student   
DEVIKA T D

  
Supervisor  
DR. SUNIL NAIR

# Acknowledgements

I express my sincere gratitude to Dr. Sunil Nair for giving me the chance to work on this project. Without his invaluable guidance, support and encouragement at every stage I would not have completed this project. I would also like to thank my group members for making the lab an ideal environment to work. I specifically thank Panja da for his constant motivation, Jitender bhayya for his help in all the analysis and life advises, Charu lady for being with me and helping me prepare for all the presentations, Avirup, Sarath, Kaustav and Deepak for all the discussions and doubt clearing sections. Rohit for giving me text books and all the ginger teas. I am grateful to Dr. Surjeet Singh for allowing me slot in PPMS. Prachi, Giri and Bag Bhayya for their cooperation and TTO measurements. Thanks a lot bag bhayya for giving valuable suggestions and guidance which were needed throughout my project. My sincere gratitude towards Dr. Ballav and his lab members for helping me with resistivity measurements. All the technical staff at  $\hbar$  especially Neelesh sir for all XRD, SEM and Reflectance measurements. Anil sir and Yatheesh sir for helping me with SEM imaging. Prasanth sir for lending me help whenever I asked. Thanks a lot Rintu, my roommate and best friend who always helped me and stood by me at all the hard and good times. Alex, Vishnu, Govind, Sreejith, Lakshmi and Meera for making my life comfortable. Visakh, Jewel and Aswin for the life talks over cup of chai. Fathima and Neenu for making me believe in myself and spreading positivity. Safeer for all inspirational-life talks, survival tips and good music. I must thank IISER for providing such good infrastructure and facilities. Vinu annan for constant support and inspiration. Last but not least Acha, Amma and Tuttukuttan for the unconditional love, support and patience.

# Abstract

Thermoelectric materials are those materials, which can directly convert a temperature difference into a useful electric energy. Looking forward to the applications of such a material, this project mainly aims at investigating naive Thermoelectric materials based on Indium and Tin. As part of the project, Indium based delafossites and Sn based perovskites were synthesized using solid state reactions and reactive flux method. The structural analysis was done by using powder XRD and SEM. The optical band gap for these materials was calculated from the Tauc's plot and thermal conductivity is measured using TTO in PPMS.  $\text{NaInO}_2$  has the least thermal conductivity and optical band gap. After analysis we chose  $\text{NaInO}_2$  as the best candidate for further doping with aim to tune its properties for a Thermoelectric material. We doped the samples with hole and electron and studied the electronic and thermal conductivity of these samples. We found that 10% & 15% doped compounds could be good thermoelectrics at high temperatures.  $\text{NaInO}_2$ , 10% & 15% doped compounds have very low thermal conductivity below room temperature, which is far less than the thermal conductivity of conventional thermoelectric materials.

# Contents

<b>1</b>	<b>Introduction</b>	<b>3</b>
1.1	Literature Survey . . . . .	5
1.1.1	Skutterudites . . . . .	5
1.1.2	Clathrates . . . . .	6
1.1.3	Half Heusler Alloys . . . . .	7
1.1.4	$\beta$ - $\text{Zn}_4\text{Sb}_3$ . . . . .	8
1.1.5	Chalcogenides . . . . .	8
1.1.6	Oxides for potential TE applications . . . . .	10
1.2	Motivation . . . . .	11
<b>2</b>	<b>Methods</b>	<b>13</b>
2.1	Synthesis . . . . .	13
2.1.1	Solid State Synthesis . . . . .	13
2.1.2	Reactive Flux route(SSR) . . . . .	13
2.2	Characterization . . . . .	14
2.2.1	X-Ray Diffraction (XRD) . . . . .	14
2.2.2	Scanning Electron Microscopy (SEM) & Energy Dispersive X-Ray Spectroscopy (EDS) . . . . .	14
2.3	Measurements of Physical Properties . . . . .	15
2.3.1	Physical Property Measurement System(PPMS) . . . . .	15
<b>3</b>	<b>Results and Discussion</b>	<b>17</b>
3.1	Indium based Delafossites & Tin based Perovskites . . . . .	17
3.1.1	Structural Analysis . . . . .	17
3.1.2	Optical Band gap . . . . .	19
3.1.3	Thermal Conductivity . . . . .	20
3.2	Doping of $\text{NaInO}_2$ . . . . .	23
3.2.1	Structural Analysis . . . . .	23
3.2.2	XRD . . . . .	23
3.2.3	Optical band gap . . . . .	24
3.2.4	Resistivity Measurements . . . . .	25
3.2.5	Thermal Conductivity . . . . .	29
3.3	Conclusion . . . . .	32
3.4	Future Plan . . . . .	33
	<b>References</b>	<b>34</b>

# Chapter 1

## Introduction

Over 60% of energy produced is wasted, and most of it is in the form of heat. Recovering a fraction of this heat by means of applying technology would be an asset to both environmental and energy needs of the humankind. One of the main issue our world is going to address in the near future is definitely the need for more varieties of multifunctional materials which could be utilized in efficient energy conversion. As a result, in the present scenario, study of Thermoelectric (TE) materials is of high importance. TE materials are those materials which directly convert thermal energy to electric energy. Thermoelectric effect is the direct conversion of a temperature difference into an electric voltage and it mainly encompasses two effects namely Seebeck effect and Peltier effect.

**Seebeck Effect:** When a temperature difference ( $\Delta T$ ) is applied at the junction of two different materials, an electric voltage ( $\Delta V$ ) is produced across the junctions.  $\frac{\Delta V}{\Delta T}$  is an intrinsic property of the material known as Seebeck coefficient ( $S$ ) [1]. Seebeck effect is the basis for thermoelectric power generation devices. (Fig 1.1)

**Peltier Effect:** When two dissimilar materials are joined together and a Current ( $I$ ) is passed through it, heat is either absorbed or emitted at the junctions. [2] This effect is due the difference in Fermi energies of the materials. The Peltier coefficient is given by  $\Pi=ST$ , where  $S$  is Seebeck coefficient,  $T$  is the temperature. Peltier effect is the basis for thermoelectric refrigeration devices. (Fig 1.1)

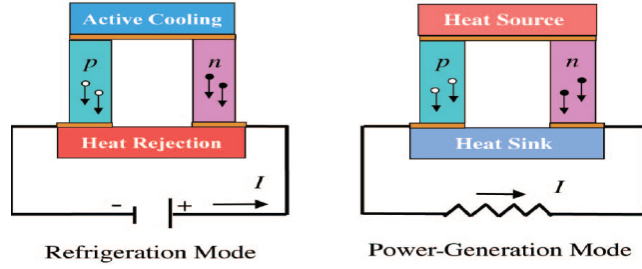


Figure 1.1: The refrigeration mode and power generation mode using TE materials, where p-, n- represents p-type and n-type semiconductors respectively. Adapted from T.M Tritt et al.[3]

Fig 1.1 shows the diagram of a Peltier thermoelectric module made of two different materials (n-type and p-type semiconductors). Depending on the configuration of the set up, one can either make a refrigeration or a power generation module. Other than the energy concerns and environmental impacts, there are more advantages for a solid state thermoelectric energy conversion. This includes compactness, localized heating or cooling and the absence of moving parts.

A material is characterized to be a potential Thermoelectric based on  $ZT$  - the dimensionless figure of merit which gives the efficiency of a TE material.

$$ZT = \frac{S^2 \times \sigma \times T}{\kappa}, \quad (1.1)$$

where  $S$  is the Seebeck Coefficient,  $\sigma$  is the electrical conductivity and  $\kappa$  is the total thermal conductivity of the material. In literature,  $Z$  and  $ZT$  are used interchangeably. Both  $Z$  &  $ZT$  specify the figure of merit of the materials at a temperature  $T$ .  $S^2\sigma$  is called as the power factor of a material which is directly proportional to the  $ZT$ , power factor is also used to mention the efficiency of a TE material. Until recent years TE materials used in devices had  $ZT \approx 1$ . In order to increase the efficiency we need materials with  $ZT > 1$ .

Electronic part of thermal conductivity  $\kappa_e$ , and electrical conductivity  $\sigma$  are interrelated to carrier concentrations  $n$  by Wiedemann-Franz law in metals. The law states that at moderate temperature the ratio of thermal conductivity to electrical conductivity is directly proportional to the temperature.

$$\frac{\kappa}{\sigma} = L_0 T, \quad (1.2)$$

where  $L_0$  is the Lorentz number. As  $ZT$  is directly proportional to electrical conductivity and inversely proportional to thermal conductivity, it is difficult to tune the power factor and figure of merit of a thermoelectric material. Fig 1.2 shows the dependence of  $S$  and  $\kappa$  on the carrier concentration. It is clear that for having a TE material with good figure of merit, one needs high  $S$ ,  $\sigma$  and low  $\kappa$ . As a matter of fact, doped semiconductors encompasses all these properties and shows maximum power factor( $S^2\sigma$ ). This makes doped semiconductors the most suitable candidates for designing a potential TE material.



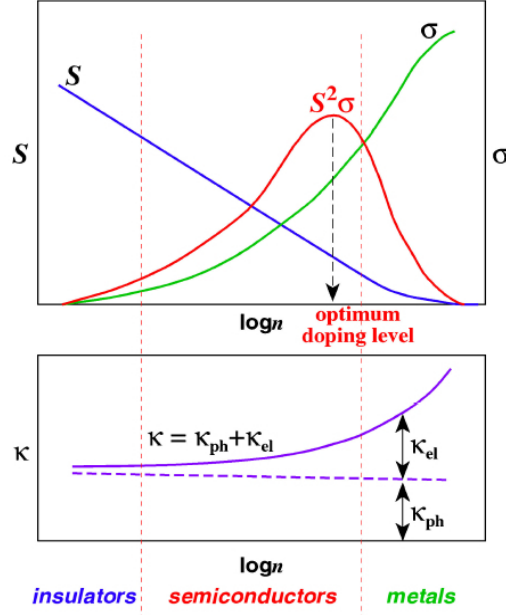


Figure 1.2: The dependence of  $S$ ,  $\sigma$  and  $\kappa$  with the carrier concentration. As the carrier concentration increases the thermal conductivity  $\kappa_e$  and  $\sigma$  is increasing and the Seebeck coefficient is decreasing. Adapted from Michitaka et al.[4]

The conventional thermoelectric materials of choice were intermetallics and alloys of heavy metals such as  $\text{PbTe}$ ,  $\text{Bi}_2\text{Te}_3$  etc. These materials have covalent bonding, which offers a carrier high mobility. Low thermal conductivity present in system along with good carrier mobility make it a good thermoelectric material. However it is difficult to commercialize thermoelectricity with these materials as they are made of heavy metals which are toxic, are not naturally abundant, have poor durability at high temperatures in air and are cost ineffective.

## 1.1 Literature Survey

As we have discussed in the introduction a good TE material should possess a low thermal conductivity and high electrical conductivity. In this section I would like to describe the recent developments in bulk TE materials and how to further modify these systems by carefully studying their physical properties.

### 1.1.1 Skutterudites

Skutterudites are Cobalt arsenide minerals ( $\text{CoAs}_3$ ) with a cubic structure. It has eight corner shared  $(\text{TX}_6)_8$  octahedra (where,  $\text{T}=\text{Co, Rh, Ir}$ ;  $\text{X}=\text{P, As and Sb}$ ). Fig 1.3 shows a typical Skutterudite framework with a large void in the center, occupying a body centered position in the cubic lattice. In these voids, large metal atoms are introduced resulting in the formation of filled Skutterudites. These guest metal atoms include lanthanides,

actinides, alkaline earth metals, alkali metals, thallium and group IV elements [5]. The composition of a filled Skutterudites can be written as  $\square_2X_8Y_{24}$ , where  $\square$  symbol shows the number of voids per unit cell,  $X = \text{Co, Rh or Ir}$ ,  $Y = \text{P, As or Sb}$ . These guest atoms introduced into the voids act as strong phonon scattering centers, thereby reducing the thermal conductivity of the system, which eventually results in improvement of TE figure of merit of these materials. [5].

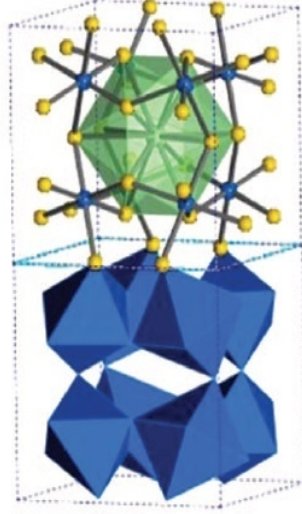


Figure 1.3: The schematic diagram of Skutterudite, where the blue dots are metal atom sites, yellow dots are pnictogen (family of Bi, Sb, As, P or N) atoms. The 12 coordinated cage in the middle shows a void, where the guest atom is introduced. Adapted from George .S .Nolas et al. [6]

The smaller and heavier metal atom as a guest in the void gives us the lowest thermal conductivity due to maximum disorder in the system. Skutterudite antimonides possess the largest voids and are of particular interest in TE applications as it can occupy comparatively large atoms in the voids [7]. At high temperatures  $\text{LaFe}_3\text{CoSb}_{12}$  and  $\text{CeFe}_3\text{CoSb}_{12}$  shows  $ZT = 1.4$ , which is a good figure of merit [8]. Small concentration of void fillers result in large reduction in thermal conductivity. In some cases, large power factor is obtained in partially filled Skutterudites in comparison with fully filled Skutterudites. In partially filled skutterudites, the voids act as electron donor which in turn helps in increasing  $ZT$ .

### 1.1.2 Clathrates

Similar to skutterudites, clathrates are also cage structured materials in which tetrahedrally bonded atoms form a framework of cages, enclosing larger metal atoms inside the voids [6]. The framework is usually made of Si, Ge and Sn. Depending on the structure clathrates can be of two types, Type I and II. Type I has  $Pm\bar{3}n$  space group and type II has  $Fd\bar{3}m$ . There are only very limited reports in literature on clathrates. Fig

1.4 shows the structure of type I & II clathrates. The general formula of type I can be written as  $X_2Y_6E_{46}$  where  $X$  &  $Y$  are guest metal atoms encapsulated in different polyhedras. Type I shows very low thermal conductivity comparable to glass-like materials, whereas Type II allows a partial filling of voids which results in high tunability of electrical conductivity in the system. These properties are highly desirable for a potential TE materials hence more investigation is required in this field.

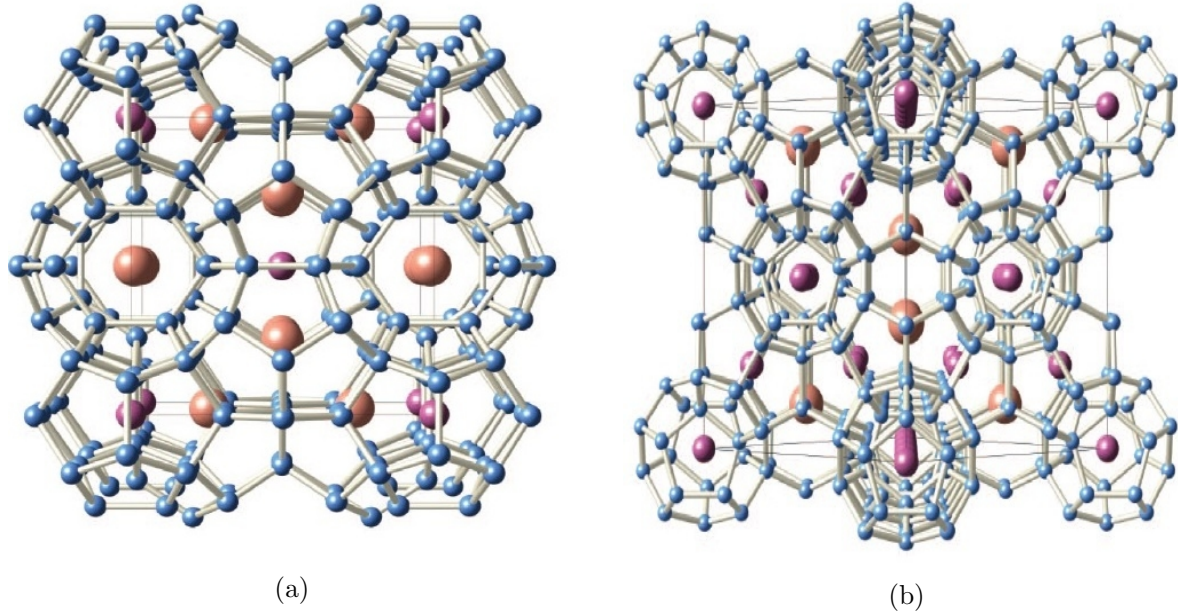


Figure 1.4: (a) Type I clathrate, the blue atoms are framework atoms, the guest atoms are shown in orange and purple in different polyhedras. (b) Type II clathrate, the blue atoms are framework atoms, the guest atoms are shown in orange and purple in different polyhedras Adapted from George.S. Nolas et al. [6].

### 1.1.3 Half Heusler Alloys

Half Heusler alloys are inter metallic alloys having chemical formula  $XYZ$ , where  $X$ ,  $Y$  and  $Z$  could be from many different groups. This class of materials have  $MgAgAs$  structure with three inter-penetrating fcc sub-lattices having  $F\bar{4}3m$  space group [9]. Fig 1.5 shows the structure of  $TiNiSn$  half Heusler (HH) alloy in which  $Ti$  and  $Sn$  occupy  $NaCl$  lattice and  $Ni$  occupies an fcc sub-lattice. In  $TiNiSn$ , doping of  $Sn$  gives electrical carriers while doping of  $Ti$  &  $Ni$  results in the mass fluctuation and there by reduced thermal conductivity. The advantage of having HH alloys as a TE material is that one can manipulate all the elements composing HH alloy to tune their properties.

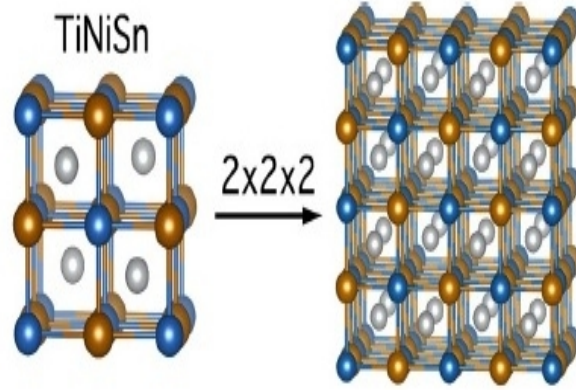


Figure 1.5: The Structure of  $TiNiSn$  alloy where, the blue atoms are Sn, metallic atoms are Ti and grey atoms are Sn. Adapted from W. Jeitschko et al. [10]

Thermoelectric HH alloys shows high room temperature Seebeck coefficient of the order of  $100\mu V K^{-1}$  [6]. So the study of HH alloys and manipulating its properties for TE materials is highly ambitious.

#### 1.1.4 $\beta$ - $Zn_4Sb_3$

Similar to HH alloys,  $\beta$  -  $Zn_4Sb_3$  is also an inter metallic material with p-type conductivity, exhibiting a maximum of  $ZT = 1.4$  at  $400^\circ C$ .  $\beta$  -  $Zn_4Sb_3$  has a hexagonal-rhombohedral crystal structure with space group  $R\bar{3}C$  and the  $\beta$  phase of  $Zn_4Sb_3$  is stable at  $263K$  -  $765K$ . The Zn atoms in the interstitials help in phonon damping, which considerably reduces the thermal conductivity. Zn also acts as an electron donor, which helps in increasing the power factor. The bonding in  $\beta$  -  $Zn_4Sb_3$  is covalent, which facilitates high carrier mobility in the system. All this characteristics sum up to a phonon-glass-electron-crystal [11] which is ideal for a good thermoelectric material. This compound is highly interesting as it has a phonon glass behavior and shows moderately high  $ZT$  [12].

#### 1.1.5 Chalcogenides

Chalcogenides is a material family comprising of a huge class of materials, most of which are semiconductors.  $Bi_2Te_3$ ,  $PbTe$ ,  $Bi_{2-x}Sb_xTe_3$  and  $Bi_2Te_{3-x}Se_x$  are some of the very famous chalcogenides from the early stages of TE investigations which are still being used in many TE applications.  $Bi_2Te_3$  shows a  $ZT$  of 0.8 to 1.0 at room temperature and on p-type doping the  $ZT$  increased to 2.4 at room temperature [13].  $PbTe$  shows a  $ZT$  of 1.5 to 1.8 at 750K and after Na doping the thermal conductivity increased to 2.2 at 950 K [14]. There are some new material compositions among chalcogenides which is getting popular these days due to its high efficiency in TE applications.  $CsBi_4Te_6$  has an anisotropic structure with mixed-valent state in Bi. By appropriate doping of  $SbI_3$  in  $CsBi_4Te_6$ ,  $ZT$  can be increased to 0.8 at 225 K [15]. This is one among the highest  $ZT$  below room temperature. There are Thallium based TE chalcogenides such as

$Tl_9BiTe_6$  &  $Tl_2SnTe_5$ , which also posses very low thermal conductivity. Tin and Antimony based thermoelectrics having general formula  $AgPb_mSbTe_{m+2}$  is another family of chalcogenides. Optimaly doped members from this family have been studied and they show  $ZT = 1.2$  to  $1.7$  at  $700$  K [16]

All the above mentioned TE materials are inter metallics which are made up of heavy metals such as Lead, Bismuth, Thallium and Antimony. These heavy metals are cost ineffective, highly toxic and rare earth materials which is not stable at higher temperatures. As a result earth abundant novel materials which are less toxic and cost effective need to be investigated.

From 1990's researchers are investigating the potential oxide TE materials, because of the increased environmental issues and to mitigate excess  $CO_2$  production. Oxides allows a higher operational temperature in air, moreover it is non toxic, cost effective and has got less environmental impact. Fig 1.6 shows the operating temperatures of TE materials investigated till date and one can find that Oxides are best choice in terms of working at higher temperatures due to its durability. The research in this field is now focusing on lowering the thermal conductivity of prospective TE materials in order to optimize  $ZT \geq 1$ .

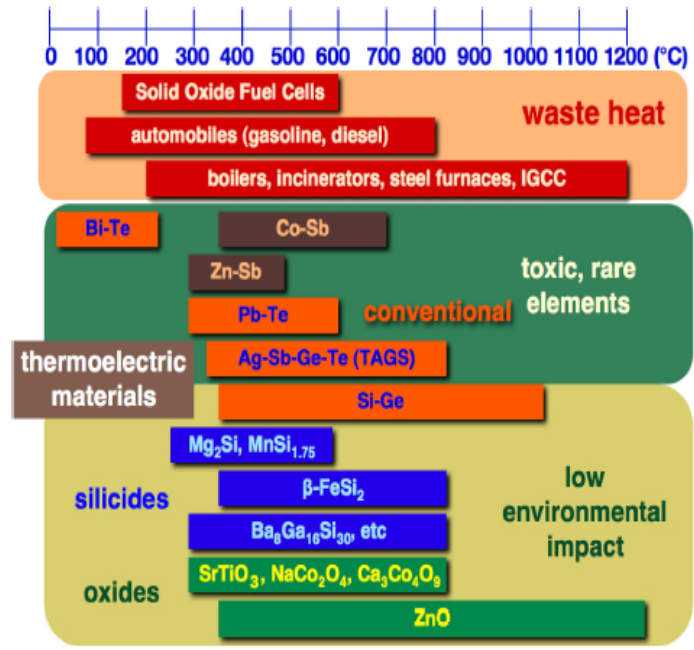


Figure 1.6: The typical source of waste heat and operating temperatures of various thermoelectric materials. Adapted from Michitaka et al.[4]

### 1.1.6 Oxides for potential TE applications

In a simple crystalline field it is difficult to manipulate the electronic and phononic system as the electrons and phonons are strongly coupled to each other. For the effective tuning of these two parameters in the system, one can take a layered structure like Delafossites. Some cobalt oxides such as  $\text{Na}_x\text{CoO}_2$ ,  $\text{Ca}_3\text{Co}_4\text{O}_9$  has layered structures, and strongly correlated electron systems in the  $\text{CoO}_2$  layers which could be effectively optimized for TE applications [17]. In a layered structure the phonon damping or scattering will be very high which in turn reduces the thermal conductivity of the system. In  $\text{Ca}_3\text{Co}_4\text{O}_9$ , it has a misfit layer, which can be looked as a hexagon on square structure, where the hexagonal  $\text{CoO}_2$  is been stacked over squared  $\text{Ca}_2\text{CoO}_3$  [18]. Fig 1.7 shows the misfit layers in  $\text{Ca}_3\text{Co}_4\text{O}_9$ , where NaCl type  $\text{Ca}_2\text{CoO}_3$  is sandwiched between  $\text{CoO}_2$ .

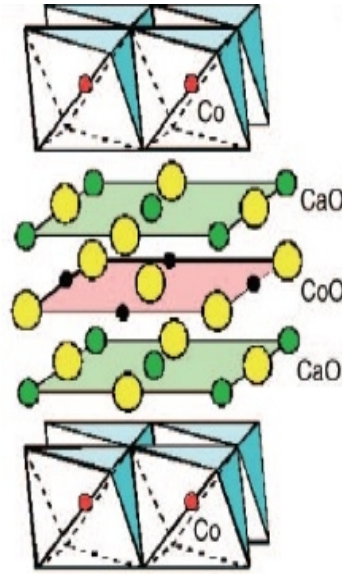


Figure 1.7: The structure of  $\text{Ca}_3\text{Co}_4\text{O}_9$  with the misfits in between the layers. Adapted from Kunihito Koumoto et al.[19]

Some reports show that Cobalt oxide layers are the most conducting oxides and at 300 K,  $\text{Ca}_3\text{Co}_4\text{O}_9$  shows comparable  $ZT$  with the conventional TE materials. The increased thermopower in  $\text{Ca}_3\text{Co}_4\text{O}_9$  is due to spin entropy present in the system [20] [21]. So far oxides were thought to have high thermal conductivity as the oxygen atom is light. It is found that this is not always true and in  $\text{Ca}_3\text{Co}_4\text{O}_9$  thermal conductivity is determined by the Cobalt atom rather than the oxygen. It is easy to tune these layered materials as potential TE materials as they have different paths for thermal current and electrical current flow in space. This help us to design the system in such a way to reduce lattice thermal conductivity by choosing an insulating block layer- this kind of a system is referred as a **phonon-glass-electron-crystal** which is ideal for TE applications [11]



## 1.2 Motivation

In this project we have mainly focused on the synthesis of Indium based delafossites and Tin based perovskites with an eye on their potential thermoelectric applications. Indium Tin Oxide (ITO) is well studied as a transparent conducting oxides, but the TE applications of these delafossites are not properly investigated. The electrically conducting samples are a good platform to start with a TE oriented study. We aim to selectively tailor the electrical and thermal conductivity of these system with electron/hole doping of these materials.

Perovskite and delafossite structures have general formula  $ABO_3$  and  $ABO_2$  respectively. A delafossite structure can be thought as A-O-A linearly coordinated layers where these layers are separated by another layer of  $BO_6$  edge sharing octahedra. Similarly in a perovskite structure  $BO_6$  octahedra is shared through the edges, where atom A, B and O occupies corners, center and face centers of a cubic lattice respectively (Fig 1.8).

By varying A and B sites of these compounds a wide variety of properties can be achieved in these systems. Tilting of  $BO_6$  octahedra in perovskites results in ferroelectricity depending on A & B site cations. From the previous studies it is known that delafossite structured compounds show electronic conductivity from insulating to metallic nature depending upon the radius of A site atoms and shows varying magnetic property depending upon the choice of B site cation [22].

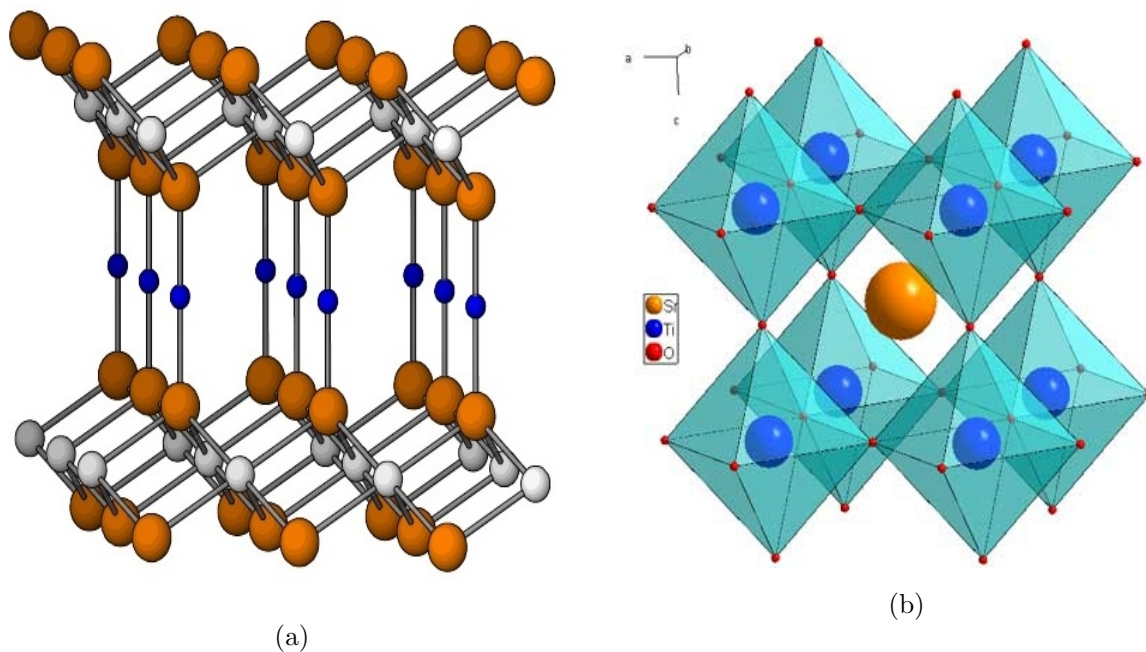


Figure 1.8: (a) Delafossite  $ABO_2$  having layered structure, where blue atoms are A, grey atoms are B and brown atoms are O in a  $ABO_2$  structure. Adapted from J.Li et al.[23]. (b) shows  $SrTiO_3$  where the brown atom in the centre is Strontium, the red atoms forming the octahedra are Oxygen and inside the oxygen octahedra blue atoms are Ti.

In perovskites there is a structural change associated with change in A & B atom. As a result many physical properties such as pyro and piezo electricity, dielectric susceptibility, linear and non linear electrooptic effects arises in these systems [24]. The layered structure present in these structures plays a crucial role in manifesting TE properties in the system by enhancing the phonon scattering and there by reducing thermal conductivity. Both In & Sn based materials are selected because these are 4-d element with electronic configuration Indium :  $[\text{Kr}] 4d^{10} 5s^2 5p^1$  and Tin:  $[\text{Kr}] 4d^{10} 5s^2 5p^2$  having high density of states which make them a good candidate for high power factor. In this project, we have tried introducing doping to these systems and to investigate their physical properties with a greater emphasis on tailoring the thermal conductivity of these systems.



# Chapter 2

## Methods

### 2.1 Synthesis

The first part of project is the sample synthesis and characterization. Solid state reaction technique or reactive flux route synthesis is used to synthesis samples at high temperature furnaces. The chemicals used as precursors were mostly from *AlfaAesar* or *Sigma – Aldrich*. Characterization of the samples were done using powder x-ray diffraction and scanning electron microscopy imaging.

#### 2.1.1 Solid State Synthesis

In solid state synthesis, the precursors were weighed according to the stoichiometric ratio and grounded well for an hour and given the temperature treatments. Each sample had a different reaction profile as shown in the table 2.1. All the samples were previously reported.

#### 2.1.2 Reactive Flux route(SSR)

In reactive flux route synthesis, one of the precursor was taken in excess amount, which facilitate as a medium for the reaction to carry out. The temperature profile is designed such that the reaction temperature is just above the melting point of the flux.

Table 2.1: Synthesis of Perovskite and Delafossites

Sample	Precursors used	Temperature(degree C)	Route	Time (hrs)
LiInO <sub>2</sub> [25]	Li <sub>2</sub> CO <sub>3</sub> , In <sub>2</sub> O <sub>3</sub>	800	SSR	16
KInO <sub>2</sub> [26]	KOH, In <sub>2</sub> O <sub>3</sub>	750	Flux	65
NaInO <sub>2</sub> [27]	Na <sub>2</sub> CO <sub>3</sub> , In <sub>2</sub> O <sub>3</sub>	900	SSR	16
CaSnO <sub>3</sub> [28]	Ca <sub>2</sub> CO <sub>3</sub> , SnO <sub>2</sub>	1400	SSR	24
SrSnO <sub>3</sub> [28]	Sr <sub>2</sub> CO <sub>3</sub> , SnO <sub>2</sub>	1400	SSR	24

Table2.1 shows the materials synthesized with their temperature profiles. The sample preparation was comparatively easy for SSR.

For the Flux route synthesis of KInO<sub>2</sub>, the flux used was KOH. Flux to the reactant

ratio was 10 : 1 [26]. As KOH is highly hygroscopic in nature, a pre-heat treatment was given for KOH at  $100^{\circ}\text{C}$ . After pre-heating, KOH and  $\text{In}_2\text{O}_3$  were weighed in 10 : 1 ratio and grounded properly for an hour in order to make it a homogeneous mixture. The mixture is then taken in a alumina crucible for the reaction at  $750^{\circ}\text{C}$ . After the reaction the excess amount of flux is removed by washing it with de-ionized water till the solvent retains a pH of 7 (neutral pH). The percentage yield for the  $\text{KInO}_2$  was 45%.

## 2.2 Characterization

### 2.2.1 X-Ray Diffraction (XRD)

For characterization of the synthesized materials, powder XRD is done for all the samples using the Bruker D8 Advance Powder X-ray Diffractometer facility available at IISER Pune, with  $\text{CuK}_{\alpha}$  radiation of wavelength 0.15406 nm as x-rays. Properly ground powder sample is mounted on to glass slide in order to take the XRD. Incident angle of x-ray is varied continuously to obtain intensity as a function of  $2\theta$ , which is recorded electronically. The intensity in arbitrary units is plotted against  $2\theta$ . Each intensity peak corresponds to a Braggs plane. The peak position can be correlated with the inter planar distance and by analyzing one can find the lattice parameters of the crystal system as well. For the preliminary analysis the intensity patterns obtained from p-xrd is matched with the data already present in International Center for Diffraction Data base(ICDD).

### 2.2.2 Scanning Electron Microscopy (SEM) & Energy Dispersive X-Ray Spectroscopy (EDS)

SEM and EDS allows us to investigate the morphology, topology of surface and composition of a given material. In SEM and EDS, a focused beam of electrons (primary electrons) are positioned on the sample of interest. This primary electrons interact differently with atoms at various depth of the samples, and as a result different emissions are produced, which includes secondary electrons, back scattered electrons, photons of characteristic X-rays etc. The secondary electrons are emitted from the top of the surface which is used to study the surface morphology and topology of the sample. These are high intensity electrons, and as a result, the image produced is of high resolution. Back scattered electrons are electron beams which are reflected from a considerable depth inside the sample by elastic scattering. The intensity of back scattered electrons is strongly related with the atomic number, as a result, it is used as an analytical tool along with the characteristic photons of X-rays. These characteristic x-rays are produced when a secondary electron is released, a higher energy electron is been filled this vacancy in the shell and releases energy. This energy released is characteristic of a particular element and thus it is used to measure the composition and abundance of a particular material.

## 2.3 Measurements of Physical Properties

### 2.3.1 Physical Property Measurement System(PPMS)

PPMS is an apparatus to investigate physical properties of a system in a temperature range of  $2K$  to  $400K$  and in a magnetic field of  $\pm 9$  Tesla. Thermal transport property of the materials are investigated using Physical Property Measurement System Evercool-II by Quantum Design.

#### Thermal Transport Measurements

Thermal conductivity is the measure of heat transport in a material, generally denoted by  $\kappa$  given as

$$\vec{j} = -\vec{\kappa} \frac{\partial T}{\partial \vec{r}}, \quad (2.1)$$

where,  $\vec{j}$  is the density of heat current flow,  $\kappa$  is the thermal conductivity and  $\frac{\partial T}{\partial \vec{r}}$  is the temperature gradient. From this equation we can see that the thermal conductivity is a random process. From kinetic energy of gases we can find the equation for thermal conductivity  $\kappa$  as

$$\kappa = \frac{1}{3} C v l, \quad (2.2)$$

where  $C$  is the specific heat of the sample,  $v$  is the particle velocity and  $l$  is the mean free path. In a 3D solid we can rewrite the above given equation as

$$\kappa = \frac{1}{3} \sum_{\alpha} C_{\alpha} v_{\alpha} l_{\alpha}, \quad (2.3)$$

where  $\alpha$  denotes all excitation which contributes to the thermal conductivity.  $\kappa$  has contribution from two parts, carrier and lattice contributions

$$\kappa_{total} = \kappa_{carrier} + \kappa_{lattice}$$

$\kappa_{carrier}$  is the thermal conductivity from the carriers like electrons and holes.  $\kappa_{lattice}$  is the thermal conductivity from lattice phonon vibrations. In metals  $\kappa_{total}$  has two carriers electron and phonons. In semiconductors, there will be hole, electron as carriers and lattice vibrations which contributes to the thermal conductivity. In insulators, lattice phonons are sole contributors to the thermal conductivity.

$$\kappa_{carrier} = \kappa_e + \kappa_h + \frac{(\sigma_e \cdot \sigma_h)}{(\sigma_e + \sigma_h)} \cdot (S_e - S_h)^2 T \quad (2.4)$$

where  $\kappa_e$ ,  $\kappa_h$  denotes thermal conductivity due to electrons and holes respectively.  $\sigma$  is the electrical conductivity, and the third term denotes the bipolar contribution towards thermal conductivity.

The lattice thermal conductivity can be written as

$$\kappa_L = \frac{1}{3} \int_0^{\frac{\theta_D}{T}} v^2 \tau_q(x) C(x) dx = \frac{1}{3} \int_0^{\frac{\theta_D}{T}} C(x) v l(x) dx \quad (2.5)$$

where,  $\tau_q$  is the phonon scattering relaxation time and  $\theta_D$  is the Debye temperature. The equation is Debye approximation for lattice thermal conductivity which is analogous to the formula derived from kinetic theory of gas.

Thermal transport measurements on sample was done using the thermal transport option(TTO) given in the PPMS. TTO can be used to measure the Thermal conductivity, thermopower and electric resistivity. For the measurement rectangular sample is wrapped in polished copper wire to make contacts. The contacts are further screwed into the gold coated shoes which serves as a thermometers, heater and a heat sink. In order to avoid outer temperature affecting the local temperature gradient in the sample the sample holder is placed inside a radiation shield. The samples dimensions were calculated. The previously made pellets were cut into rectangular shape using a crystal cutter to avoid any unevenness in the surface and cross sections. The dimensions were noted down using a digital vernier.

### Resistivity Measurements

Resistance of the samples are measured using a four probe method, in which KEITHLEY model no.6221 (current source) and KEITHLEY model no.2182A (Nanovoltmeter) were employed. Generally in any resistivity measurements an electric current is passed through the sample and voltage drop across the sample is recorded. The samples were all pellets and for a good contact between the probe and the sample silver paste was used. All measurements were done at room temperature.

### Reflectivity Measurements

Reflectance is the fraction of incident light which is reflected back from the material. PerkinElmer Lambda 950 UV/Vis spectrophotometer is used to do the Reflectivity measurements for the samples. The sample is made into the form of a pellet and used the solid state set up of PEL 950 spectrophotometer to do the measurements which has a range of wavelength from 150 nm to 3300 nm wavelength. Deuterium-Quartz tungsten lamp is used to provide such a wide range of wavelength. There is one integrating sphere attached with solid state set up which helps in directing all signals towards the detector thus it has a high sensitivity at lower intensities also. Reflectivity is an important phenomenon in terms of tuning optical properties in transparent conducting oxides. From the Reflectivity measurements one can find the optical band gap of a material using Tauc's relationship  $\alpha h\nu \propto (h\nu - E_g^{opt})^{\frac{n}{2}}$  [29] where,  $\alpha$  is the absorption coefficient,  $h$  is the Plank's constant,  $\nu$  frequency of light,  $E_g^{opt}$  is the optical band gap and  $n$  is an integer which gives the allowed optical transition number.

# Chapter 3

## Results and Discussion

### 3.1 Indium based Delafossites & Tin based Perovskites

From the literature, we now know that for an efficient thermoelectric we need materials with lower thermal conductivity and high electric conductivity. In this thesis we are investigating a few Indium based delafossites and Tin based perovskites for TE properties. Samples were synthesized using SSR and Flux route synthesis. Structural, physical properties of the systems were studied using XRD, PPMS, Four Probe, and UV/Vis Spectrophotometer

#### 3.1.1 Structural Analysis

##### XRD patterns

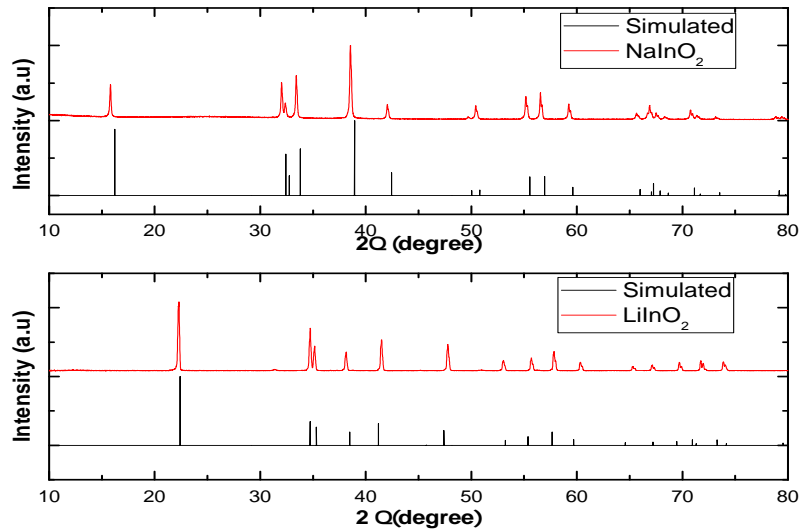


Figure 3.1: The powder XRD pattern for LiInO<sub>2</sub> and NaInO<sub>2</sub> with the reference pattern, both the samples are phase pure.

The structure and composition of all synthesized materials were analyzed using powder x-ray diffraction patterns. The ICDD basis was used to index the peaks and compare the XRD patterns obtained from sample. The delafossite structures  $\text{LiInO}_2$ ,  $\text{KInO}_2$ ,  $\text{NaInO}_2$  have tetragonal, rhombohedral and trigonal structures respectively. The perovskite structures  $\text{CaSnO}_3$  and  $\text{SrSnO}_3$  have orthorhombic and cubic structure respectively. All the samples were phase pure. Fig 3.1 and Fig 3.2 shows the powder XRD pattern of the materials synthesized along with the reference patterns. All these samples were previously reported and our results were consistent with them [25]-[28]

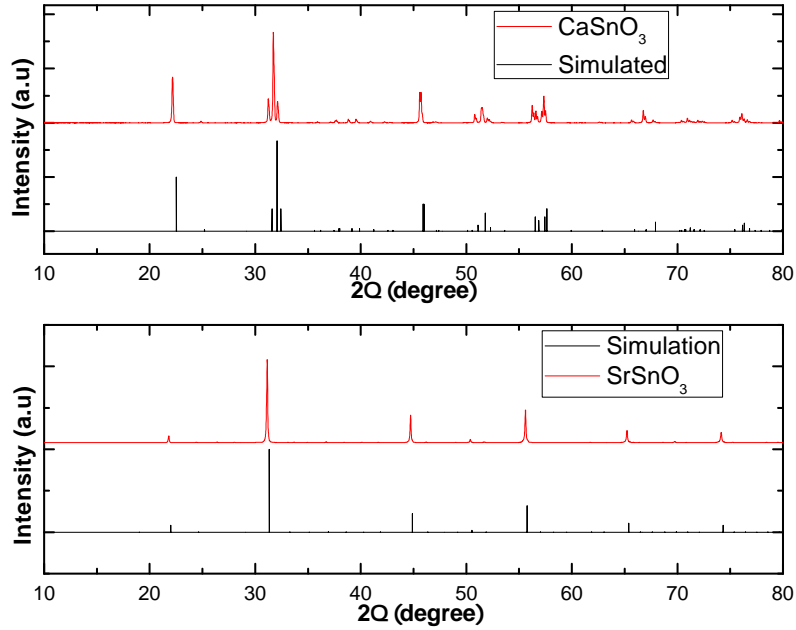


Figure 3.2: The powder XRD pattern for  $\text{CaSnO}_3$  and  $\text{SrSnO}_3$  along with the reference pattern, showing that both the samples are phase pure.

Table 3.1: The lattice parameters and crystal systems of Delafossites and perovskites.

Compound	a	b	c	$\alpha$	$\beta$	$\gamma$	Crystal System
$\text{LiInO}_2$	4.312	4.312	4.312	90	90	90	Tetragonal
$\text{NaInO}_2$	3.23	3.23	16.398	90	90	120	Trigonal
$\text{KInO}_2$	3.29	3.29	18.322	90	90	120	Trigonal
$\text{CaSnO}_3$	5.661	7.88	5.661	90	90	120	Trigonal
$\text{SrSnO}_3$	4.039	4.039	4.039	90	90	90	Orthorhombic

### 3.1.2 Optical Band gap

From reflectance data, using Tauc's equation [29], optical band gap of each material has been calculated Fig 3.3, table 3.2 shows the optical band gaps of the samples synthesized.

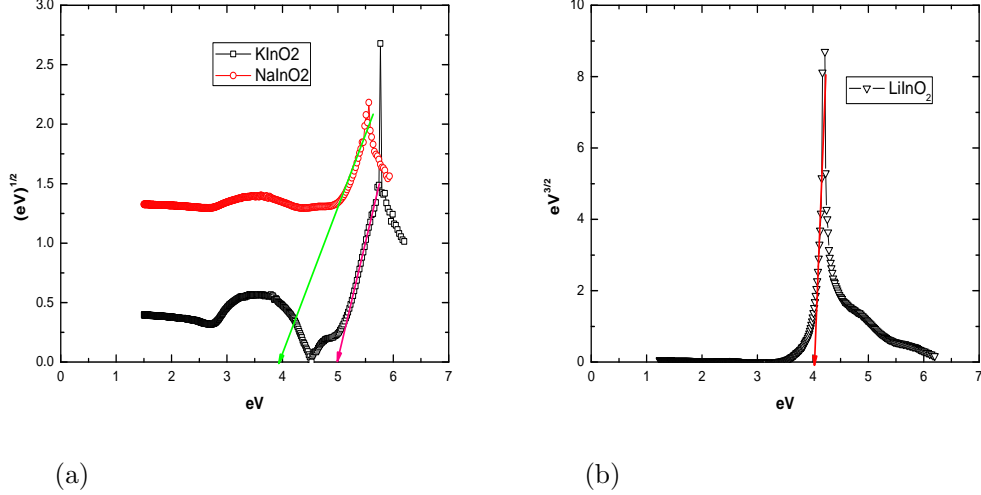


Figure 3.3: Optical band gaps of In based delafossites figure (a)  $\text{NaInO}_2$  and  $\text{KInO}_2$  (b)  $\text{LiInO}_2$

The reflectivity of samples were measured in a wavelength range of 200-800 nm and the band gap values were calculated from these data using Tauc's relationship [29] which is given as.

$$\alpha h\nu \propto (h\nu - E_g^{opt})^{\frac{n}{2}} \quad (3.1)$$

where,  $\alpha$  is the absorption coefficient. From the above equation one can find the band gap by plotting  $(\alpha h\nu)^{\frac{n}{2}}$  versus  $h\nu$  and extrapolating it to zero.  $(\alpha h\nu)^{\frac{n}{2}}$  is calculated from the reflectivity measurements, where  $n$  is an integer which can take  $n=1,3,4,6$  according to the characteristics of optical transitions [30]. This can be thought as directly allowed, directly forbidden, indirectly allowed and indirectly forbidden optical transitions for  $n=1,3,4,6$  respectively.

Fig3.3 shows the optical band gap of delafossite samples synthesised. The  $\text{KInO}_2$  and  $\text{NaInO}_2$  have directly allowed optical transitions with  $n=1$ .  $\text{LiInO}_2$  has a directly forbidden optical transition with  $n=3$ . The calculated band gap values were consistent with the reported literature [31]. The multiple transition seen in 3.3(a) is due to other 4d transitions occurring in the system.  $\text{CaSnO}_3$  and  $\text{SrSnO}_3$  are having directly allowed and indirectly allowed optical transitions respectively with  $n=1$  and  $n=4$  3.4. These results were also consistent with previously reported literature [30].

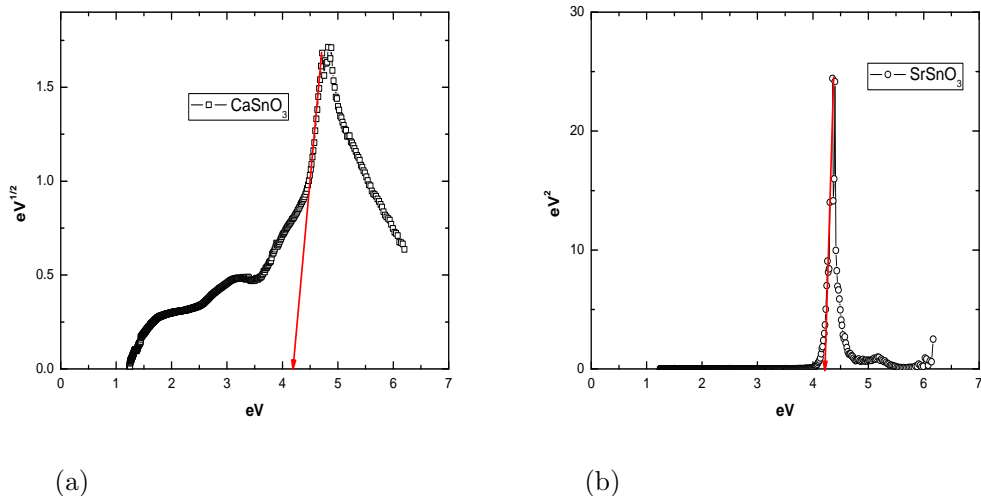


Figure 3.4: Optical band gaps of Sn based Perovskites figure (a) shows  $\text{CaSnO}_3$ , (b)  $\text{SrSnO}_3$  respectively.

Table 3.2: The optical band gap of perovskites and delafossites synthesized

	Material	Bandgap (eV)
(A)	$\text{LiInO}_2$	4.0
(B)	$\text{NaInO}_2$	4.0
(C)	$\text{KInO}_2$	5.0
(D)	$\text{CaSnO}_3$	4.2
(E)	$\text{SrSnO}_3$	4.1

The optical band gap of delafossite structures and perovskite structures synthesized is given in table 3.2. In Indium based compounds  $\text{NaInO}_2$  and  $\text{LiInO}_2$  have same band gap with with directly allowed and directly forbidden transitions. In Tin based compounds  $\text{SrSnO}_3$  and  $\text{CaSnO}_3$  have the comparable band gap. Among all these materials  $\text{KInO}_2$  has the highest band gap.

### 3.1.3 Thermal Conductivity

The thermal conductivity of samples were measured in the PPMS from 4K to 300K. For the measurement the samples were cut into small rectangular specimens and contacts were made on them using copper wire and silver paste.

$\text{LiInO}_2$  shows a maximum thermal conductivity with a phonon peak Fig3.5. The phonon peak is a trade mark of crystalline materials. According to Debye's approximation in lower temperatures the thermal conductivity shows a  $T^3$  behavior, and at higher temperatures (till room temperature) the thermal conductivity follows a  $T^{-1}$  dependence. In the lower temperatures the thermal conductivity is dominated by boundary process,



after a particular temperature the thermal conductivity will be dominated by phonon - phonon scattering. This change in domination in the thermal conductivity will give rise to the phonon peak in thermal conductivity. The temperature at which this peak is observed is typically known as the crossover temperature [32]. The phonon-phonon scattering in a crystal lattice is known as umklapp process or U process, which limits the thermal conductivity of a system at higher temperatures.

We have used Debye approximation for lattice thermal conductivity to fit this data, which takes care of the U-process also. All samples followed power law in the lower temperature regime 4K to 60K for delafossite structures. Linear dependence of  $\text{LiInO}_2$ ,  $\text{KInO}_2$  and  $\text{NaInO}_2$  is  $T^{2.09}$ ,  $T^{1.72}$  and  $T^{2.065}$  respectively. The deviation of thermal conductivity from  $T^3$  law, is attributed to the strong interaction between electrons and phonons in the lower temperatures [33].

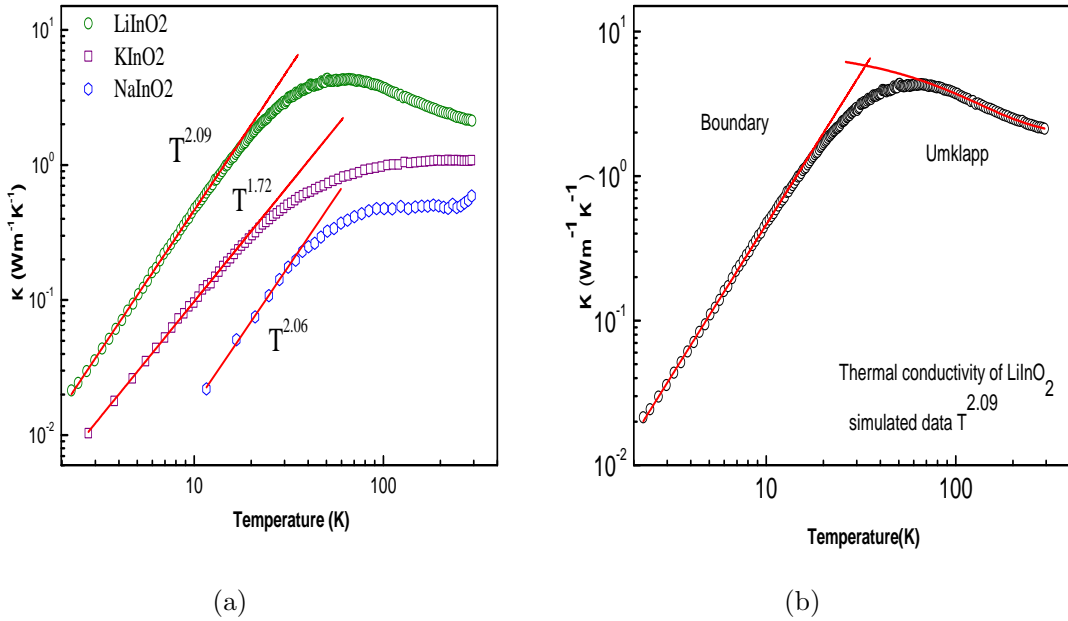


Figure 3.5: Thermal conductivity of In- based delafossites (a) shows the thermal conductivity of In- based delafossites, where  $\text{NaInO}_2$  has the lowest thermal conductivity. (b) Thermal conductivity of  $\text{LiInO}_2$  with the phonon peak is shown.

The perovskites also show a linear dependence of thermal conductivity at low temperature regime. The dependence was almost equal for both the perovskite systems,  $\text{CaSnO}_3$ ,  $\text{SrSnO}_3$  showed  $T^{1.96}$  and  $T^{1.97}$  respectively Fig3.6.

In glass and other amorphous materials, between 4K & 20K the thermal conductivity is independent of temperature. This is because of the Rayleigh scattering which results in a sudden decrease in the phonon mean free path [34].

Except in  $\text{LiInO}_2$ , all other samples showed glass like behavior at a much higher temperature or immediately after the cross over temperature. We can look it as a quasi crystalline behavior. From the cross over temperature till 300K the thermal conductivity of each sample except  $\text{LiInO}_2$  is independent of temperature Fig3.5. At 300K the thermal conductivity of  $\text{NaInO}_2$  tend to increase, due to the increase in  $\kappa_e$  with the temperature [35].

In comparison with the other synthesized materials, the thermal conductivity of  $\text{NaInO}_2$  is the least. In delafossite systems, the U process starts dominating at 60 K, due to which the thermal conductivity either decreases or tend to remains constant and shows a typical glass like plateau. In perovskite systems, the U process starts dominating from 80 K. At 60 K the thermal conductivity of  $\text{LiInO}_2$ ,  $\text{NaInO}_2$ , and  $\text{KInO}_2$  is 4.28, 0.34 and 0.84 ( $\text{Wm}^{-1}\text{K}^{-1}$ ). In perovskite the maximum thermal conductivity is 0.98 ( $\text{Wm}^{-1}\text{K}^{-1}$ ) for  $\text{CaSnO}_3$  and for  $\text{SrSnO}_3$  the thermal conductivity is 2.20 ( $\text{Wm}^{-1}\text{K}^{-1}$ ) Fig3.6.

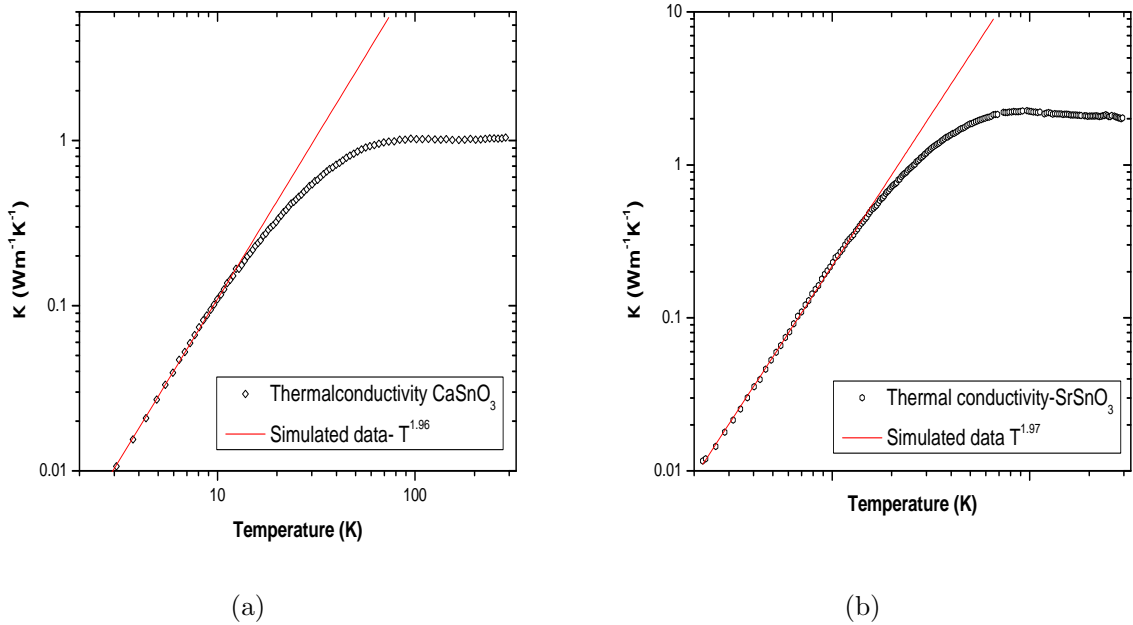


Figure 3.6: Thermal conductivity of Sn- based perovskites, at the lower temperatures a linear dependence and at higher temperatures a temperature independent plateau is seen. (a) Thermal conductivity of  $\text{CaSnO}_3$ , showing  $T^{1.96}$  dependence. (b) Thermal conductivity of  $\text{SrSnO}_3$ , showing  $T^{1.97}$  dependence

From the optical band gap measurements and thermal conductivity measurements, we found that among all the materials synthesized  $\text{NaInO}_2$  is the best choice for a TE material with lowest of the thermal conductivity and direct optical transition (4.0 eV and  $0.34 \text{ Wm}^{-1}\text{K}^{-1}$ ) from these materials. Therefore we chose  $\text{NaInO}_2$  for further hole and electron doping.

## 3.2 Doping of NaInO<sub>2</sub>

In order to tune NaInO<sub>2</sub> properties for a potential TE material, both electron and hole doping can be attended. In this study Cadmium (Cd<sup>2+</sup>), Tin(Sn<sup>4+</sup>) were doped at In<sup>3+</sup> position as electrons and holes respectively. NaIn<sub>1-x</sub>A<sub>x</sub>O<sub>2</sub>, where x=0.05, 0.10, 0.15 is synthesized using solid state route as mentioned earlier.

### 3.2.1 Structural Analysis

### 3.2.2 XRD

The p-type doping of transparent oxide delafossites is not an easy task. Intrinsic defects and compatibility in solubility is present in most of the transparent conducting oxides and delafossite systems which limits doping [36]. While doping hole (Sn<sup>4+</sup>) in NaInO<sub>2</sub>, due to limited solubility high concentration of Sn<sup>4+</sup> doped sample were not phase pure, the impurity is identified as In<sub>2</sub>O<sub>3</sub> one of the precursor material. During the analysis we found that till 15% hole and electron doping there is no change in the symmetry and space group of the material, but there is a variation in the lattice parameter Table 3.3. The detailed analysis of structure by doing Rietveld refinement need to be carried out.

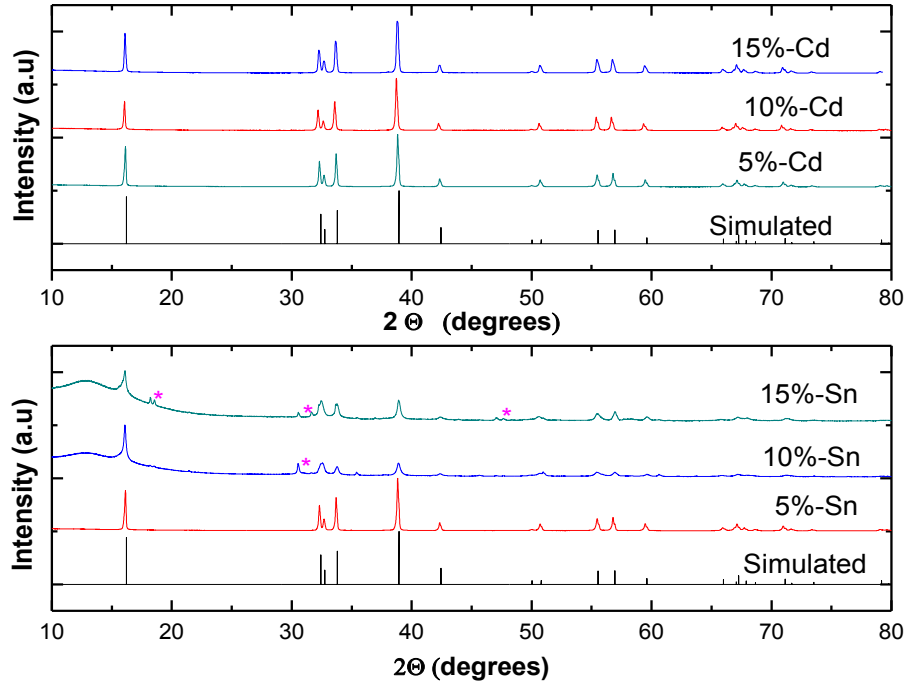


Figure 3.7: shows the powder XRD pattern for phase pure Cadmium doped NaInO<sub>2</sub>. The impurity peaks of In<sub>2</sub>O<sub>3</sub> in Tin doped NaInO<sub>2</sub> is marked\*

Using Le-Bail refinement the lattice parameters of the samples were calculated. On doping the lattice parameters a,b were constant for all concentrations of doping and there was a change in c. Table3.3 shows the variation in the lattice constant c, with the doping.

Table 3.3: The lattice constant  $c$  ( $\text{\AA}$ ), for all the doped samples, along with parent compound

sample	0%	5%	10%	15%
Cd- $\text{NaInO}_2$	16.398	16.378	16.351	16.360
Sn- $\text{NaInO}_2$	16.398	16.376	16.401	16.411

The lattice constants a,b was same for all compounds 3.230 but c varied for the doped samples.

### 3.2.3 Optical band gap

The optical band gap of materials were calculated using the Tauc plot, from the reflectivity measurements. In  $\text{NaInO}_2$  as the doping increases the band gap reduced. This behavior was expected in any doped material. For electron and hole doping at particular concentrations the band gap of materials were comparable.

Table 3.4: The band gaps(eV) of compounds with different concentration of hole and electron doping

	15%	10%	5%	0%
Sn- doped $\text{NaInO}_2$	2.8	2.9	3.1	4.0
Cd- doped $\text{NaInO}_2$	2.8	2.8	2.9	4.0

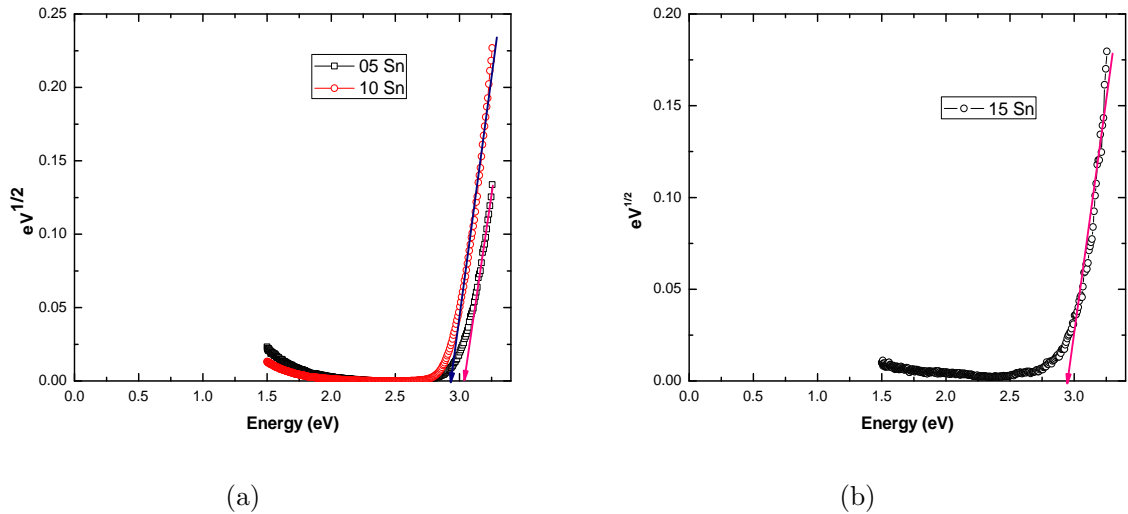


Figure 3.8: (a) Optical band gap of 10 & 5% Sn doped  $\text{NaInO}_2$ , (b) Optical band gap of 15% Sn doped  $\text{NaInO}_2$  is shown. As the doping increases, optical band gap decreases.

In comparison with the parent compound, electron & hole doped samples showed a highly reduced band gap. This is usual in any doped systems. 15% & 10% doped samples showed almost equal band gaps in both electron and hole doped systems.

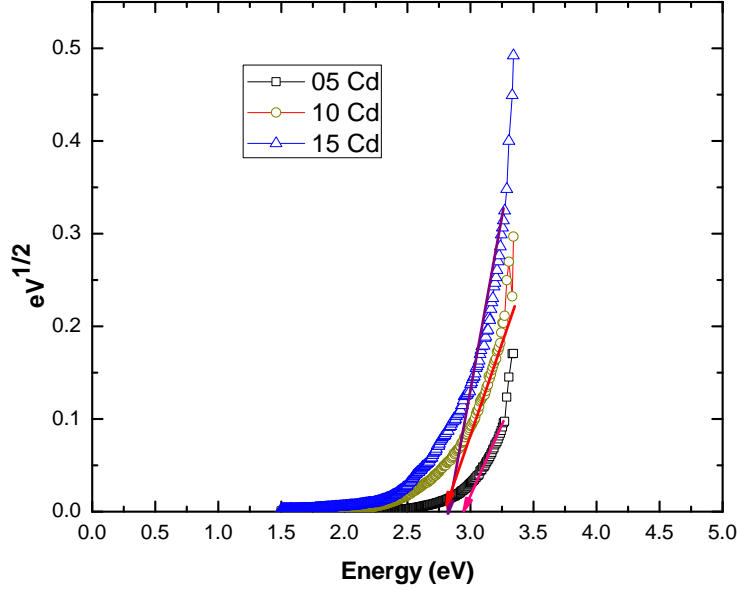


Figure 3.9: The optical band gap of hole doped  $\text{NaInO}_2$ , 15% & 10% Cd doped samples have comparable band gap.

### 3.2.4 Resistivity Measurements

The resistivity of all doped samples have been measured using a four probe set up at room temperature. For making good contacts with the probes silver paste was used. The following equation were used in order to calculate the resistivity of materials

$$\rho_o = 2\pi \cdot S \cdot V/I \quad (3.2)$$

$$\rho = \rho_o \times 1/G \quad (3.3)$$

$$G = \frac{W/S}{2 \ln \left( \frac{\sinh(W/S)}{\sinh(W/2S)} \right)} \quad (3.4)$$

$$(3.5)$$

where, S is the probe distance in the four probe set up, W is thickness of the sample, and G is the sample dimension consideration for a pellet.

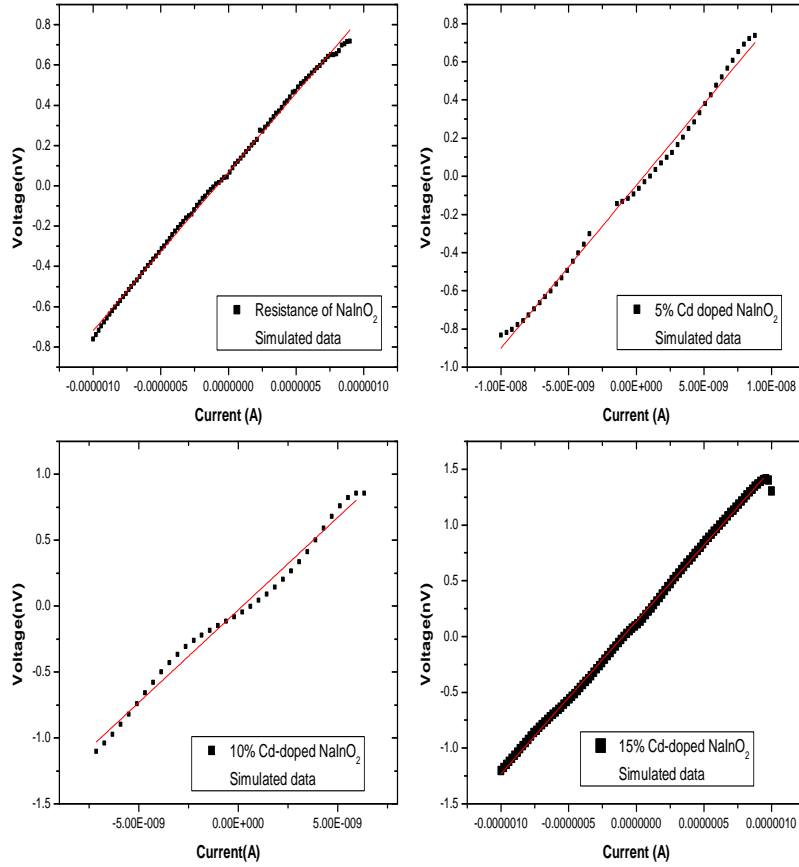


Figure 3.10: shows the room temperature resistance of Cd- doped  $\text{NaInO}_2$  along with the parent compound

Table 3.5: Showing resistance in ( $\Omega\text{m}$ ) for all the  $\text{NaInO}_2$  based systems

Sample	0%	5%	10%	15%
Cd- $\text{NaInO}_2$	$3.6 \times (10^3)$	$3.4 \times (10^5)$	$8.6 \times (10^3)$	$7.7 \times (10^3)$
Sn- $\text{NaInO}_2$	$3.6 \times (10^3)$	$3.1 \times (10^5)$	$6.4 \times (10^3)$	$4.3 \times (10^3)$

There is conductivity anomalies seen in electron and hole doped samples from the un-doped samples. Un-doped  $\text{NaInO}_2$  showed more conductivity than the 5% doped samples. However the conductivity of 10% and 15% doped samples were higher than the parent compound. The conductivities of 10% and 15% doped samples were comparable, which is in good agreement with the optical band gap measurements.

It is unclear that why there is a higher conductivity for un-doped sample than the doped samples. As the measurement taken was a crude one, we need to look upon this data and come up with a better way of measurements. In previous reports similar results has been discussed with doped *Cr* based delafossites [38]. It is proposed that this anomaly due to the inappropriate mixing of 4d orbitals in the doped samples. As the doping increases the sample tries to retain the proper mixing. To comment further on this anomaly one has to do a detailed band gap analysis of these samples.

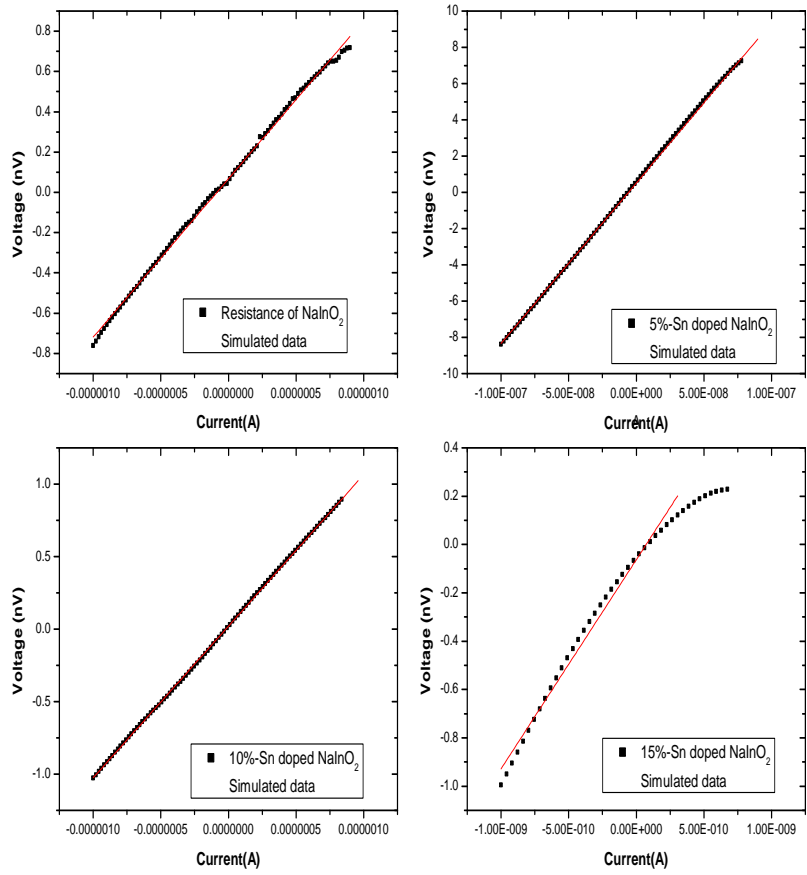


Figure 3.11: shows the room temperature resistance of Sn- doped  $\text{NaInO}_2$  along with the parent compound

From the resistivity data of samples conductivity of sample is calculated. Fig3.12 shows the conductivity of  $\text{NaInO}_2$  samples at room temperature. As the doping concentration increased the electrical conductivity of the system is also increased due to increase in the number of carriers.

Table 3.6: The electronic conductivity (S/cm) for all the NaInO<sub>2</sub> samples.

Amount of doping	Cd- NaInO <sub>2</sub>	Sn- NaInO <sub>2</sub>
0%	2.7E-7	2.7E-7
5%	2.9E-8	3.2E-8
10%	1.16E-6	1.56E-6
15 %	1.29E-6	2.32E-6

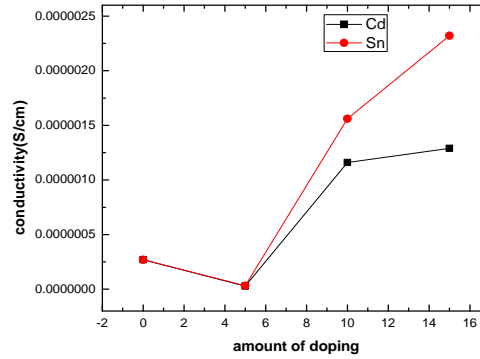


Figure 3.12: The room temperature conductivity of doped NaInO<sub>2</sub> along with the parent compound, one can easily notice that there is a dip in the conductivity of 5% hole doped and electron doped samples



### 3.2.5 Thermal Conductivity

With doping of electron and hole, the thermal conductivity of the samples increased. This can be attributed to the increased carrier mobility of the system upon doping. In comparison among doped systems, the effect of carrier-phonon interaction was more in electron doped systems. As a result the electron doped samples showed a lower conductivity and a comparatively smaller temperature dependence in the lower temperatures. As In(Z=49), Cd(Z=48) and Sn(Z=50) all have comparable masses, the phonon scattering due to mass fluctuation is ineffective. The doped samples also showed a thermal conductivity plateau. At the cross over temperature, the thermal conductivity of doped samples were much higher than that of parent compound.

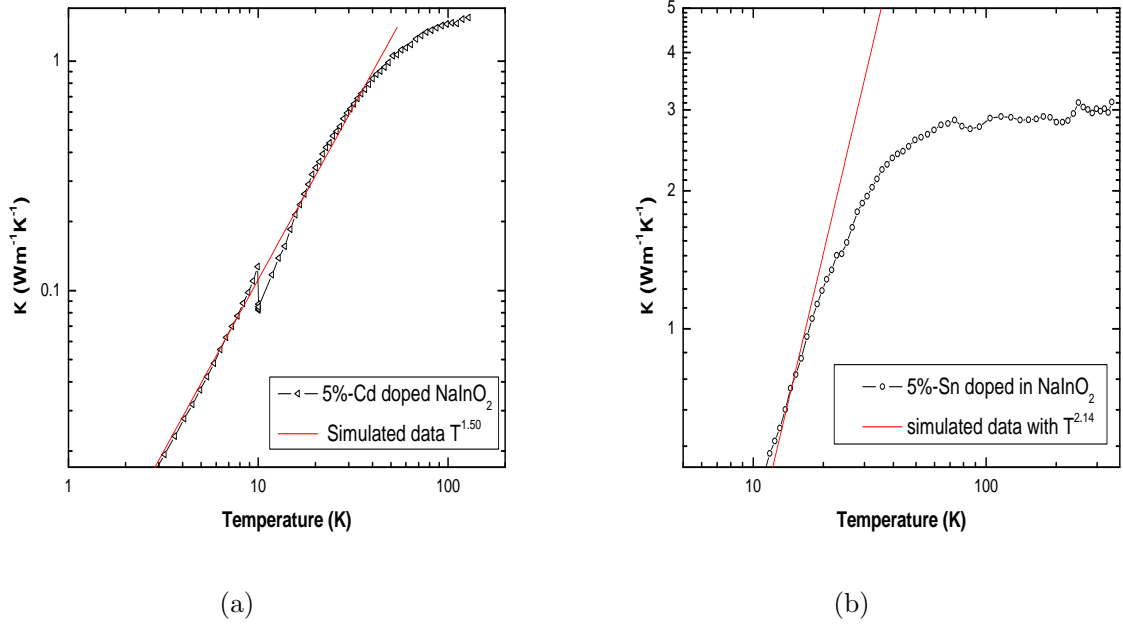


Figure 3.13: (a) Thermal conductivity of 5% electron doped  $\text{NaInO}_2$  with temperature dependence of  $\kappa$  being 1.58. (b) The thermal conductivity of 5% hole doped  $\text{NaInO}_2$  with temperature dependence of  $\kappa$  being 2.14.

Fig 3.13 shows the thermal conductivity and temperature dependence of 5% hole doped and electron doped  $\text{NaInO}_2$ . The temperature dependence of  $\text{NaIn}_{0.95}\text{Cd}_{0.05}\text{O}_2$  is  $T^{1.58}$  and  $\text{NaIn}_{0.95}\text{Sn}_{0.05}\text{O}_2$  is  $T^{2.14}$ . From this we can say that at lower temperatures the lattice phonon and electron interaction is much stronger in the electron doped samples [33]. As the intensity of interaction increases there is a more deviation from the  $T^3$  dependence. Both the samples showed a temperature thermal conductivity plateau which corresponds to a quasi crystalline behavior [34]. The value of thermal conductivity at the characteristic plateau for  $\text{NaIn}_{0.95}\text{Cd}_{0.05}\text{O}_2$  is  $1.45 \text{ WK}^{-1}\text{m}^{-1}$  and for  $\text{NaIn}_{0.95}\text{Sn}_{0.05}\text{O}_2$  is  $2.6 \text{ WK}^{-1}\text{m}^{-1}$ . As the phonon-electron interactions is stronger than the phonon-hole interactions the

5% hole doped sample shows a higher thermal conductivity than the 5% electron doped sample.

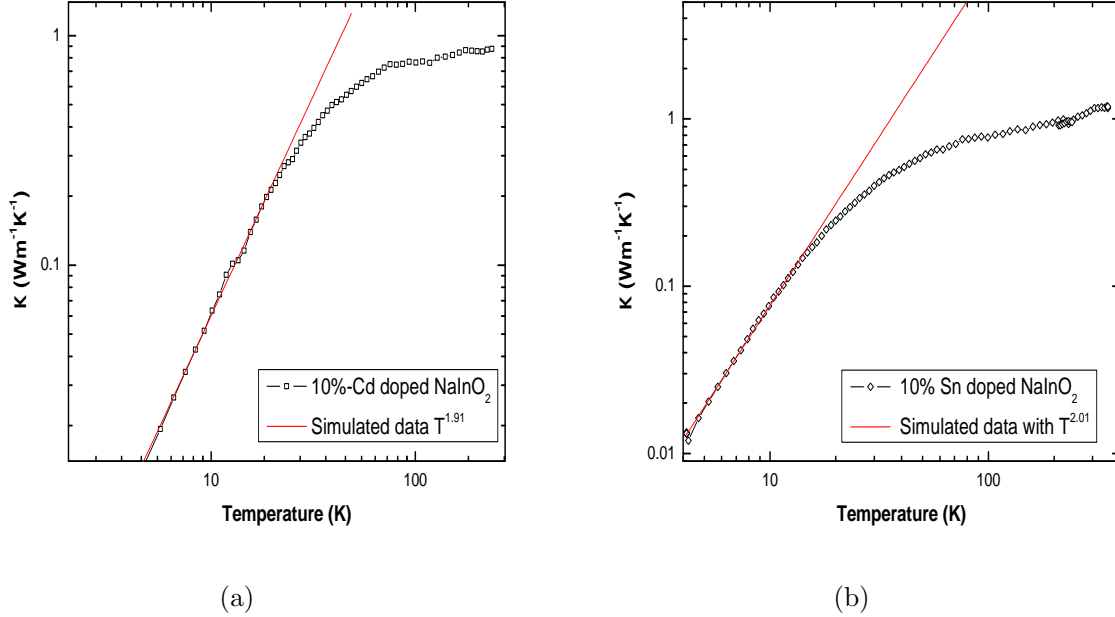
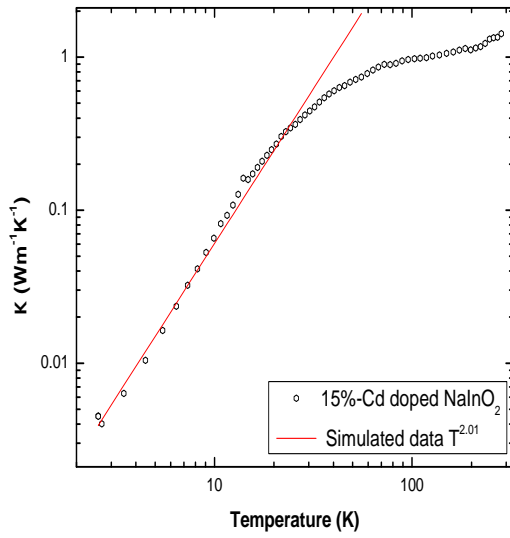


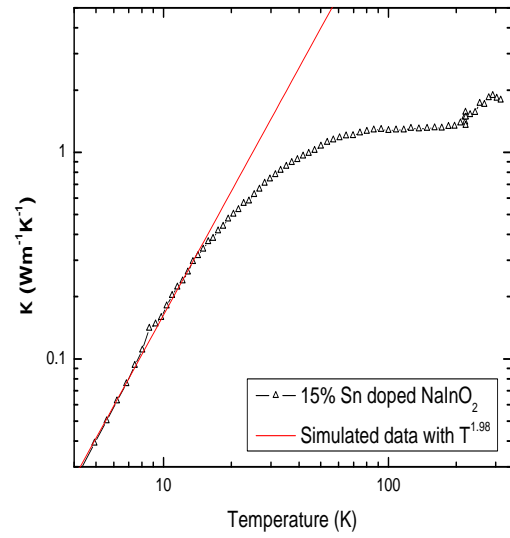
Figure 3.14: (a) Thermal conductivity of 10% electron doped NaInO<sub>2</sub> with the temperature dependence of  $\kappa$  being 1.91. (b) Thermal conductivity of 10% hole doped NaInO<sub>2</sub> with temperature dependence of  $\kappa$  being 2.01

The 10% doped samples also showed a linear dependence in the lower temperatures and a characteristic quasi crystalline behavior at a much higher temperature. The temperature dependence and the thermal conductivity in both electron doped and hole doped samples were comparable. NaIn<sub>0.90</sub>Cd<sub>0.10</sub>O<sub>2</sub> showed a temperature dependence of  $T^{1.91}$  and thermal conductivity 0.73 WK<sup>-1</sup>m<sup>-1</sup>. NaIn<sub>0.90</sub>Sn<sub>0.10</sub>O<sub>2</sub> have a slightly higher temperature dependence of  $T^{2.01}$  and thermal conductivity 0.77 WK<sup>-1</sup>m<sup>-1</sup>. In comparison the phonon-electron scattering is more in 10% Cd doped samples and as a result the temperature dependence and thermal conductivity is comparatively less for this sample.

The trend showed an anomaly in 15% hole and electron doped samples. The temperature dependence and thermal conductivity of the hole doped sample found to be less than that of electron doped sample. Both the samples have a linear dependence on the thermal conductivity in the lower temperatures and characteristic quasi crystalline thermal conductivity plateau at higher temperatures Fig3.15. The thermal conductivity of NaIn<sub>0.85</sub>Cd<sub>0.15</sub>O<sub>2</sub> is .94 WK<sup>-1</sup>m<sup>-1</sup> with a temperature dependence of  $T^{2.01}$ . NaIn<sub>0.85</sub>Cd<sub>0.15</sub>O<sub>2</sub> showed a temperature dependence of  $T^{1.98}$  and thermal conductivity 1.27 WK<sup>-1</sup>m<sup>-1</sup>.



(a)



(b)

Figure 3.15: (a) Thermal conductivity of 15% electron doped  $\text{NaInO}_2$  with temperature dependence of  $\kappa$  being 2.014. (b) Thermal conductivity of 15% hole doped  $\text{NaInO}_2$  with temperature dependence of  $\kappa$  being 1.98

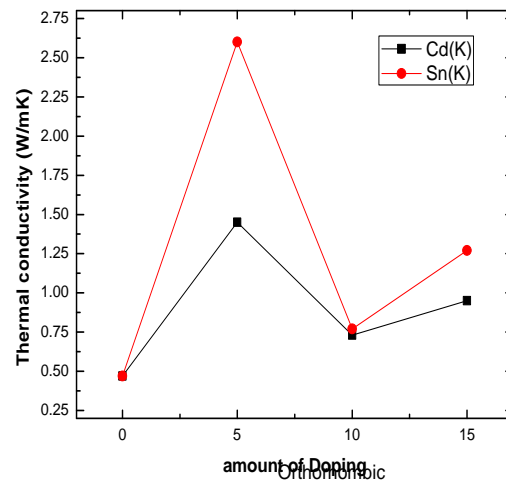


Figure 3.16: The thermal conductivity for different doping concentration is shown, 10% doped samples shows optimal thermal conductivity for a TE material among the doped compounds.

The thermal conductivity of parent compound is less than that of the doped samples,

this is because of the increase in carrier mobility by doping. As the doping concentration increases the thermal conductivity decreases due to strong phonon electron interactions and increased phonon scattering. [39]. In general the hole doped samples showed more thermal conductivity than the electron doped samples.

### 3.3 Conclusion

In this project we have synthesized three delafossites and two perovskites namely  $\text{LiInO}_2$ ,  $\text{NaInO}_2$ ,  $\text{KInO}_2$ ,  $\text{CaSnO}_3$  and  $\text{SrSnO}_3$ . Among these materials we found that  $\text{NaInO}_2$  is a best choice for a potential thermoelectric material as it has the least thermal conductivity and lowest optical band gap.  $\text{NaInO}_2$  is further doped with electron ( $\text{Cd}^{2+}$ ) hole ( $\text{Sn}^{4+}$ ) with an eye on improving its thermoelectric properties. The optical band gap, room temperature conductivity and thermal conductivity of these samples have measured and found that 15% hole and electron doped samples showed the maximum electrical conductivity. 10% hole and electron doped samples showed least thermal conductivity, but this thermal conductivity values are comparable with 15% doped samples. The thermal conductivity values of  $\text{NaInO}_2$ , 10% and 15% of hole and electron doped samples are much less than the conventional thermoelectric materials.

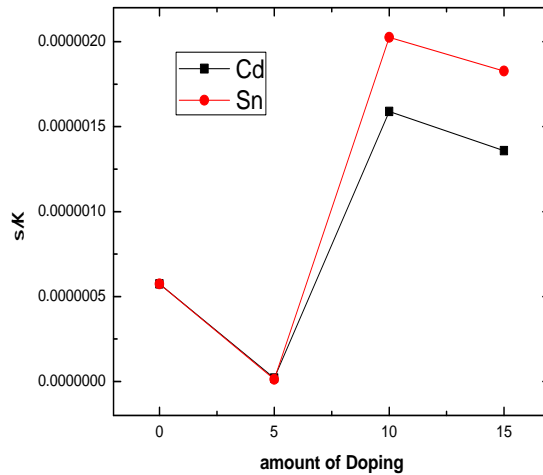


Figure 3.17: The ratio of  $\sigma$  to  $\kappa$  is plotted against the concentration of doping.

At higher temperatures this samples could be possibly viable thermoelectric materials. Fig3.17 shows the plot between  $\sigma/\kappa$  and concentration of doping. This will give us an idea about the goodness of samples as thermoelectric material as  $ZT$  is directly proportional to  $\sigma/\kappa$ . From the Fig3.17 we can see that 10% doped sample is optimally doped for thermoelectric applications.

## 3.4 Future Plan

1. Rietveld refinement and structural analysis of all the samples synthesized.
2. High temperature thermopower, and all  $ZT$  measurements of 10% doped samples.

# References

- [1] T. J. Seebeck, *Abhandlungen der Kniglich Preussischen Akademie der Wissenschaften* 18 (1821) 371.
- [2] J. C. Peltier, *Annales de Chimie et de Physique* 56 (1834) 371.
- [3] T. M. Tritt, M. A. Subramanian, *MRS Bulletin* 31 (2006) 188–198. doi:10.1557/mrs2006.44, [link].  
URL [http://journals.cambridge.org/article\\_S088376940000991X](http://journals.cambridge.org/article_S088376940000991X)
- [4] M. OHTAKI, *Journal of the Ceramic Society of Japan* 119 (1395) (2011) 770–775. doi:10.2109/jcersj2.119.770.
- [5] G. S. Nolas, D. T. Morelli, T. M. Tritt, *Annu. Rev. Mater. Sci* 29 (1999) 89.
- [6] G. S. Nolas, J. Poon, M. Kanatzidis, *MRS Bulletin* 31 (2006) 199–205. doi:10.1557/mrs2006.45, [link].  
URL [http://journals.cambridge.org/article\\_S0883769400009921](http://journals.cambridge.org/article_S0883769400009921)
- [7] , 15<sup>th</sup> international conference on thermoelectrics, 15<sup>th</sup> international conference on thermoelectrics (1999) 91.
- [8] B. C. Sales, D. Mandrus, R. K. Williams, *Science* 272 (5266) (1996) 1325–1328. arXiv:<http://science.sciencemag.org/content/272/5266/1325.full.pdf>, doi:10.1126/science.272.5266.1325, [link].  
URL <http://science.sciencemag.org/content/272/5266/1325>
- [9] W. Jeitschko, *Metallurgical Transactions A* 1 (1970) 3159–3162.
- [10] J. E. Douglas, P. A. Chater, C. M. Brown, T. M. Pollock, R. Seshadri, *Journal of Applied Physics* 116 (16). doi:<http://dx.doi.org/10.1063/1.4900497>, [link].  
URL <http://scitation.aip.org/content/aip/journal/jap/116/16/10.1063/1.4900497>
- [11] G. A. Slack, *The CRC handbook of Thermoelectrics*, CRC Press, 1995.
- [12] G. J. Snyder, M. Christensen, E. Nishibori, T. Caillat, B. B. Iversen, *Nat Mater* 3 (7) (2004) 458–463. doi:10.1038/nmat1154, [link].  
URL <http://dx.doi.org/10.1038/nmat1154>
- [13] C. B. Satterthwaite, R. W. Ure, *Phys. Rev.* 108 (1957) 1164–1170. doi:10.1103/PhysRev.108.1164, [link].  
URL <http://link.aps.org/doi/10.1103/PhysRev.108.1164>
- [14] K. Biswas, J. He, I. D. Blum, C.-I. Wu, T. P. Hogan, D. N. Seidman, V. P. Dravid, M. G. Kanatzidis, *Nature* 489 (7416) (2012) 414–418. doi:10.1038/nature11439, [link].  
URL <http://dx.doi.org/10.1038/nature11439>
- [15] D.-Y. Chung, T. Hogan, P. Brazis, M. Rocci-Lane, C. Kannewurf, M. Bastea, C. Uher, M. G. Kanatzidis, *Science* 287 (5455) (2000) 1024–1027. doi:10.1126/science.287.5455.1024.

- [16] A. Majumdar, *Science* 303 (5659) (2004) 777–778. arXiv:<http://science.sciencemag.org/content/303/5659/777.full.pdf>, doi:10.1126/science.1093164, [link].  
URL <http://science.sciencemag.org/content/303/5659/777>
- [17] M. Mikami, S. Ohtsuka, M. Yoshimura, Y. Mori, T. Sasaki, R. Funahashi, M. Shikano, *Japanese Journal of Applied Physics* 42 (6R) (2003) 3549. [link].  
URL <http://stacks.iop.org/1347-4065/42/i=6R/a=3549>
- [18] T. Itoh, I. Terasaki, *Japanese Journal of Applied Physics* 39 (12R) (2000) 6658. [link].  
URL <http://stacks.iop.org/1347-4065/39/i=12R/a=6658>
- [19] K. Koumoto, I. Terasaki, R. Funahashi, *MRS Bulletin* 31 (2006) 206–210. doi:10.1557/mrs2006.46, [link].  
URL [http://journals.cambridge.org/article\\_S0883769400009933](http://journals.cambridge.org/article_S0883769400009933)
- [20] Y. Wang, N. S. Rogado, R. J. Cava, N. P. Ong, Spin entropy as the likely source of enhanced thermopower in  $\text{NaCo}_2\text{O}_4$ , *Nature* 423 (6938) (2003) 425–428. doi:10.1038/nature01639.  
URL <http://dx.doi.org/10.1038/nature01639>
- [21] W. Koshibae, K. Tsutsui, S. Maekawa, *Phys. Rev. B* 62 (2000) 6869–6872. doi:10.1103/PhysRevB.62.6869, [link].  
URL <http://link.aps.org/doi/10.1103/PhysRevB.62.6869>
- [22] M. A. Marquardt, N. A. Ashmore, D. P. Cann, *Thin Solid Films* 496 (1) (2006) 146 – 156, proceedings of the Fourth International Symposium on Transparent Oxide Thin Films for Electronics and Optics (TOEO-4) Proceedings of the Fourth International Symposium on Transparent Oxide Thin Films for Electronics and Optics (TOEO-4). doi:<http://dx.doi.org/10.1016/j.tsf.2005.08.316>, [link].  
URL <http://www.sciencedirect.com/science/article/pii/S0040609005015038>
- [23] C. J. B. T. J. Li, A.W. Sleight, *Journal of Solid State Chemistry* 178 (2005) 285–294.
- [24] A. M. GLAZER, *Acta Cryst A* 31 (1975) 756.
- [25] S. Kawakami, M. Sasaki, H. Tabata, H. Shimooka, S. Kohiki, S. Matsushima, M. Oku, T. Shishido, *Journal of Alloys and Compounds* 359 (12) (2003) 278 – 280. doi:[http://dx.doi.org/10.1016/S0925-8388\(03\)00179-8](http://dx.doi.org/10.1016/S0925-8388(03)00179-8), [link].  
URL <http://www.sciencedirect.com/science/article/pii/S0925838803001798>
- [26] M. Bharathy, Q. Zhao, H.-C. zur Loye, *Journal of Crystal Growth* 312 (23) (2010) 3533 – 3535. doi:<http://dx.doi.org/10.1016/j.jcrysgro.2010.08.039>, [link].  
URL <http://www.sciencedirect.com/science/article/pii/S0022024810005816>
- [27] S. M. M. O. T. H. T. W. S. T. Kouichi Fukuzaki, Shigemi Kohiki, H. Shimooka, *Journal of Materials Chemistry* 10 (2000) 779–782.
- [28] O. P. Shail Upadhyay, *Journal Of Material Science Letters* 16 (1997) 13301332.
- [29] T. et al., *Phys. Status Solidi* 15 15 (1966) 627.
- [30] W. Zhang, J. Tang, J. Ye, gh, *Journal of Materials Research* 22 (2007) 1859–1871. doi:10.1557/jmr.2007.0259.  
URL [http://journals.cambridge.org/article\\_S0884291400025413](http://journals.cambridge.org/article_S0884291400025413)

- [31] J. W. Lekse, B. J. Haycock, J. P. Lewis, D. R. Kauffman, C. Matranga, The effect of electronic structure changes in naino2 and nain0.9fe0.1o2 on the photoreduction of methylene blue, *J. Mater. Chem. A* 2 (2014) 9331–9337. doi:10.1039/C4TA00906A.
- [32] R. Berman, *The Thermal Conduction in Solids*, Oxford University Press, New York, 1976.
- [33] J. Yang, D. T. Morelli, G. P. Meisner, W. Chen, J. S. Dyck, C. Uher, , *Phys. Rev. B* 65 (2002) 094115. doi:10.1103/PhysRevB.65.094115.  
URL <http://link.aps.org/doi/10.1103/PhysRevB.65.094115>
- [34] J. L. Cohn, G. S. Nolas, V. Fessatidis, T. H. Metcalf, G. A. Slack, *Phys. Rev. Lett.* 82 (1999) 779–782. doi:10.1103/PhysRevLett.82.779, [link].  
URL <http://link.aps.org/doi/10.1103/PhysRevLett.82.779>
- [35] T. M. Tritt, *Thermal Conductivity- Theory Properties and Application*, year =.
- [36] X. Nie, S.-H. Wei, S. B. Zhang, *Phys. Rev. Lett.* 88 (2002) 066405. doi:10.1103/PhysRevLett.88.066405, [link].  
URL <http://link.aps.org/doi/10.1103/PhysRevLett.88.066405>
- [37] S. B. Zhang, S.-H. Wei, A. Zunger, Microscopic origin of the phenomenological equilibrium “doping limit rule” in *n*-type iii-v semiconductors, *Phys. Rev. Lett.* 84 (2000) 1232–1235. doi:10.1103/PhysRevLett.84.1232.  
URL <http://link.aps.org/doi/10.1103/PhysRevLett.84.1232>
- [38] R. Nagarajan, A. D. Draeseke, A. W. Sleight, J. Tate, *Journal of Applied Physics* 89 (12).
- [39] C. Uher, J. Yang, S. Hu, D. T. Morelli, G. P. Meisner, *Phys. Rev. B* 59 (1999) 8615–8621. doi:10.1103/PhysRevB.59.8615, [link].  
URL <http://link.aps.org/doi/10.1103/PhysRevB.59.8615>